The effect of hydrogen dilution on the structure of a-C:H

1998 J. Phys.: Condens. Matter 10 4161

(http://iopscience.iop.org/0953-8984/10/19/004)

J. Phys.: Condens. Matter **10** (1998) 4161–4176. Printed in the UK PII: S0953-8984(98)89857-3

The effect of hydrogen dilution on the structure of a-C:H

J K Walters†, R J Newport‡, S F Parker§, W S Howells§ and G Bushnell-Wye‖

† Department of Physics and Astronomy, University College London, Gower Street, London WC1E 6BT, UK
‡ Physics Laboratory, The University, Canterbury, Kent CT2 7NR, UK
§ ISIS Facility, CLRC Rutherford Appleton Laboratory, Didcot, Oxon OX11 0QX, UK
‖ CLRC Daresbury Laboratory, Daresbury, Warrington WA4 4AD, UK

Received 8 December 1997

Abstract. Two a-C:H samples were prepared using a fast-atom deposition system from acetylene and an acetylene/hydrogen gas mixture. Their structure was investigated using neutron and x-ray diffraction and infrared spectroscopy measurements. Compositional analysis shows that a 1:1 C_2H_2:H_2 mixture results in a change from a-C_{77}:H_{23} to a-C_{79}:H_{21}, i.e. has a very small effect on the composition. The diffraction data also show that the addition of hydrogen to the precursor gas has no significant effect on the average bond distances and angles but shows a small change in the H–C–H and C–C–H correlations between the two samples. However, the infrared data show that there are significant changes in the bonding of hydrogen within the sample—changes which do not affect the average network structure. We observe a decrease in the amount of sp^3 CH_2 and CH_3 groups, and an increase in the fraction of sp^2 and sp^3 CH groups, with the formation of a second sp^2 CH bonding environment in the hydrogen-diluted sample. Therefore, in addition to providing useful structural information on these a-C:H samples, this set of experiments illustrates very well the complementary nature of the data from diffraction and spectroscopic techniques.

1. Introduction

A complex problem in the study of amorphous materials is that of determining the relationship between its atomic-scale structure and its macroscopic properties, the solution of which maintains amorphous materials in a position of both fundamental and technological interest.

An example of such a material is amorphous hydrogenated carbon (a-C:H). It is of technological interest because it can be prepared in such a way that it is harder, denser and more resistant to chemical attack than any other solid hydrocarbon [1, 2] which, together with a high degree of transparency to the infrared and histocompatibility, has led to many applications [3, 4]. The macroscopic properties of this material depend critically on the conditions under which it is prepared [5]: forms of a-C:H vary from the soft, polymeric form (high hydrogen content with many $–CH_2–$ chains) at one extreme and the graphitic form (high sp^2 carbon content, low hydrogen content) at the other. Hard or 'diamond-like' a-C:H forms under conditions of intermediate deposition energies, which result in a large degree of cross-linking and structural rigidity, and an intermediate hydrogen content.

Important points to have emerged from our work on a-C:H with intermediate hydrogen concentrations include the fact that we find a C–C:C=C ratio of around 3:1, with hydrogen

0953-8984/98/194161+16$19.50

having a preference to bond to sp^3 carbon. The $CH:CH_2$ ratio is found to be $\sim$1:1, with a preference for sp^3 CH/CH_2 and with rather little CH_3 present; we have also provided the first unambiguous evidence for molecular H_2, trapped in oblate spheroidal cages within the a-C:H network [6]. There is evidence from NMR [7] for some medium-ranged H-density fluctuations, namely that sp^3 C–H is associated with short (<5 carbons) chains whilst elsewhere there is a mixture of sp^3 C–H and sp^2 C–H in regions separated from the sp^3 chains by a layer, at least one carbon atom thick, of non-protonated carbon. However, perhaps the single most important piece of work centres on the demonstration by means of neutron diffraction (and supported by NMR and molecular dynamics simulation) that the C=C double bonds are almost exclusively olefinic in nature—this observation alone was enough to require that the structural models accepted hitherto (which invoke relatively large clusters of aromatic/graphitic sp^2/π bonding, interlinked by sp^3/σ hybridized carbons) be rejected in their existing form [8].

Complementary high-resolution diffraction and infrared spectroscopy data are necessary to study the subtle changes in structure associated with variations in deposition parameters, as studied here. For instance, the effective deposition energy is already known to be a crucial parameter in determining the properties and overall structure of the deposited film [9–12]. Also, the effective impact energy at the growth volume is dependent on the spectrum of fragment sizes derived from the source and, therefore, on the nature of the precursor gas and, of course, on the physical processes involved in the ionization/decomposition processes associated with this method of deposition. The basis of models currently used to relate deposition parameters to the structure of the deposited material is the 'subplantation' model of Lifshitz *et al* [10] (and expounded in the a-C:H context by Robertson [13]). In the 'subplantation' model, growth of the film occurs via the following steps.

(i) Penetration by the bombarding species in the target matrix.
(ii) Stopping of the energetic species in the target matrix.
(iii) Occupation of a site in the host matrix.
(iv) Internal subsurface growth.
(v) Change in the surface composition.
(vi) Determination of the film structure.

The penetration depth, trapping efficiency and distribution in the target material depend on the type and energy of the bombarding species and the nature of the target material. Also some of the bombarding species may be reflected and therefore do not contribute to the growth of the film directly, but may transfer energy to the target atoms. Once the impinging species have penetrated the target surface, energy loss occurs by three principal mechanisms: atomic displacements, phonon excitations and electron excitations. These mechanisms can play a significant role in determining the final structure of the film. Also, simultaneous with these film growth mechanisms, processes are occurring which contribute to 'erosion' of the evolving film, e.g. collisional and chemical sputtering.

The effect of diluting the precursor gas with hydrogen has been investigated directly for a-C:H [9, 14]; however, much more work has been done on its effect on the structure of a-Si:H [15] and other a-Si alloys [16–18]. Hydrogen dilution of the precursor gas during the deposition of these materials was first carried out with a view to enhancing their electronic properties, particularly for the improved performance of solar cells [16]. According to Alvarez *et al* [19], the motivation for hydrogen dilution is to cover the growing surface with hydrogen to increase the mobility of the adsorbed species, thereby producing a more relaxed structure. This seems to work for high dilution levels (>80%) where improved film homogeneity, reduced microvoid fractions and reduced di/polyhydride configurations

are consistently observed [15, 16, 19]—all are characteristic of a more relaxed structure. However, at lower dilution levels this is not necessarily the case, and for a-Si:H, some workers report an increase in di/polyhydride bonding conformations [15]. In all cases, hydrogen dilution results in a decrease in the film deposition rate [16–18].

Our own studies of the effects of 30% hydrogen dilution on the structure of a-Si:C:H [20] show an overall increase in the hydrogen content of the sample and an increase in the number of SiH_2 groups, relative to SiH, with hydrogen dilution.

The effect of hydrogen dilution on the structure of a-C:H has not been well studied [9, 14], although it is known that the presence of hydrogen is essential for diamond film production from CH_4 in CVD processes [21]. In fact, little is known about the role of hydrogen in the deposition process in general. It is important in chemical etching of material from the growth region [10, 13] and has often been thought of as a means of stabilizing sp^3 carbon bonds [4, 22]. In the discussion of these new results, we hope to be able to add further insight into the involvement of hydrogen in the deposition mechanism.

Building on our previous work, we present complementary neutron and x-ray diffraction and infrared spectroscopy data for a-C:H samples with and without hydrogen dilution of the precursor gas. This information will be used to provide additional insight into the carbon and hydrogen bonding environments present in a-C:H, with reference to our revised model structure, and to examine the effects of hydrogen dilution on the atomic-scale structure of the material.

Diffraction experiments provide an opportunity for obtaining direct information on interatomic distances and on the average numbers of atoms in each coordination shell. Neutron diffraction has already been established as a powerful technique in the study of amorphous materials (see, for example, [23–25]), and in particular the pulsed neutron source ISIS at the Rutherford Appleton Laboratory (UK) allows one to obtain high-resolution real-space data, to the extent that it is possible to distinguish sp^1, sp^2 and sp^3 carbon bonding environments directly [23]. Furthermore, because the neutron, unlike x-rays or electrons, scatters from the nucleus, there is no atomic-number-dependent form factor and the correlations involving hydrogen are also accessible. Conversely, this fact may be exploited in x-ray diffraction where it is possible to obtain a pair distribution function which highlights the correlations which do not involve hydrogen.

IR spectroscopy is a widely used technique in the study of these materials (see, e.g., [26–28]), especially for investigating the hydrogen bonding environment. Previously, Dischler *et al* [26] performed an extensive study of the bonding of hydrogen in a-C:H, and proposed assignments for all of the observed frequencies. Also, Vandentrop *et al* [28] used IR spectroscopy to estimate CH_2:CH_3 ratios, but all IR results necessarily depend upon assumptions for the matrix elements of each vibration, making fully quantitative analysis very difficult. However, the technique has been used quite successfully to look at trends among different samples [29, 30].

So, a combination of these two experimental methods, diffraction (average bond lengths and angles) and IR (frequencies and relative peak intensities) enables the relative proportions of different bonding environments to be determined with a higher degree of reliability.

2. Experimental details and data analysis

2.1. Sample preparation and analysis

The samples were prepared using a saddle-field fast-atom (i.e. neutral-particle) source [31, 32] from acetylene and hydrogen precursor gases at a deposition pressure of

Table 1. Compositional information.

Sample	Mass flow ratio of precursor gases acetylene:hydrogen	C content (at.%)	H content (at.%)	Beam energy (eV)	Density (g cm^{-3})	Number density (atoms Å^{-3})
1	1:0	77	23	$\sim$ 800	1.6	0.1
2	1:1	79	21	$\sim$ 800	1.6	0.1

$\sim 10^{-4}$ mbar. Hydrogen gas was simply fed into the source with the acetylene at a 1:1 mass flow ratio. Both the samples were prepared at an effective energy of 800 eV, with the substrate at room temperature. The conditions for each sample deposition were identical apart from the added hydrogen in the precursor gas: the mass flow rate of acetylene was the same for both. These experiments require samples in the form of powders and this is achieved by depositing the thin films onto a copper substrate, previously cleaned by etching with Ar. Since copper carbide does not form readily, the stresses in the thin film soon cause it to detach from the substrate, and as it falls the powder sample is collected. The compositions of the samples were determined by Carlo–Erba CHN combustion analysis. The bulk density was measured using a conventional residual-volume method; this tends to underestimate the microscopic density (which is the value estimated or inferred from plasmon loss measurements) for samples having microvoids. The results of these measurements, together with the deposition energies used, are summarized in table 1.

2.2. Neutron diffraction

The data presented here were collected using the SANDALS diffractometer [33] at the pulsed neutron facility, ISIS, at the Rutherford Appleton Laboratory (UK). This instrument is particularly well suited to the study of covalently bonded amorphous materials, allowing the collection of data over a wide dynamic range ($\sim$0.2–50 Å^{-1}). It is also optimized for looking at hydrogenous samples by collecting data only at forward-scattering angles to reduce the effects of inelastic scattering. This is discussed more fully in the data analysis section of the paper.

Neutrons are scattered from the sample into fixed angle detectors (i.e. at a given scattering angle 2θ), where the scattered intensity is measured as a function of time of flight (tof), which can be directly related to momentum transfer. The complete scattering profile is then obtained by combining overlapping spectra from different detector angles. Monitors record the tof spectra of the incident and transmitted beams to provide information on the total neutron cross-section and the intensity:wavelength profile of the incident beam. For each experiment measurements are required for: the sample, the empty sample container, a background without sample or container and a vanadium rod of comparable geometry to the sample and container. The vanadium rod measurement allows the sample scattering to be put on an absolute scale, since vanadium has a well-known and almost entirely incoherent scattering cross-section [34].

In a neutron scattering experiment the aim is to determine a structure factor, $S(Q)$, where, for an amorphous material (i.e. an isotropic scatterer) [34],

$$S(Q) = 1 + \frac{4\pi\rho}{Q}\int_0^\infty r\ \mathrm{d}r\ [g(r) - 1]\sin(Qr) \tag{1}$$

where ρ is the average number density of atoms in the material, $Q = |\boldsymbol{Q}| = |\boldsymbol{k}_i - \boldsymbol{k}_f|$ is the wavevector transfer associated with the diffraction experiment—for elastic scattering

from a liquid or amorphous solid, $Q = (4\pi/\lambda)\sin\theta$, where 2θ is the scattering angle and λ is the neutron wavelength—and $g(r)$ is called the pair correlation function. $g(r)$ is a measure of the atomic density at a distance r from a given origin atom. The pair correction function may be obtained by Fourier transformation of the structure factor, which is directly related to the measured neutron scattering intensity. For a binary system such as a-C:H, there are contributions to the total structure factor from each atom-type pair, i.e. there are six independent contributions which are weighted to give the total structure factor. The corresponding real-space function, the total pair correlation function, $G(r)$, is a weighted combination of the partial pair correlation functions, and is defined (according to the Faber–Ziman formalism [34]) as

$$G(r) = \sum_{\alpha\beta}[c_\alpha c_\beta b_\alpha b_\beta g_{\alpha\beta}(r)] \tag{2}$$

where c_α is the atomic fraction and b_α the coherent scattering length respectively, of element α; and where $g_{\alpha\beta}(r)$ represent the partial terms in $G(r)$, and describe the probability of finding an atom of type β at a distance r from an atom of type α at the origin.

The equations above rely on the static approximation [35, 36] being valid, i.e. that the change in the neutron's energy on scattering is small compared to its incident energy. Corrections need to be applied to the data before a structure factor can be generated. The major corrections are for background, container and multiple scattering, attenuation and the effects of inelastic scattering. Full details of these may be found elsewhere [37]. The most problematic step in the analysis procedure is the correction for inelastic scattering. Although the SANDALS instrument has been designed to minimize the effects of this on the experimental data, it is by no means completely eliminated and still has to be corrected for. For hydrogenous materials the simplistic approaches [38] to accounting for this deviation from purely elastic scattering (i.e. deviations from the static approximation) break down because of the low mass and high incoherent cross-section of the hydrogen atom, and an alternative method has to be found. The method adopted here is an empirical one which involves fitting a low-order polynomial through the data to remove the underlying incoherent scattering curve; to first order the effects of inelastic scattering are embedded in this term. The procedure for performing this correction is given in detail elsewhere [39]. There are problems with using this approach, particularly with regard to the quality of the data associated with hydrogen correlations at very low r-values (below $\sim$1 Å) which may affect correlation amplitudes. Therefore, we expect peak intensities, and to a far lesser extent bond distances, for correlations involving hydrogen first coordination shells to be subject to larger uncertainties than pertain to the bulk of the data. Also, note that hydrogen has a negative neutron scattering length, so C–H and C–C–H correlations will appear as negative-going features in the $G(r)$ function.

2.3. X-ray diffraction

The data presented here were obtained using standard flat-plate (θ:2θ) transmission diffraction geometry [40] on Station 9.1 at the Daresbury Laboratory Synchrotron Radiation Source, Warrington (UK). Measurements are taken of the sample and of the empty sample cell. The windows of the sample cell are made of Kapton which has a well-known, weak and relatively featureless diffraction pattern. Also, the sample is rotated constantly during the experiment to minimize errors arising from possible variations in sample thickness. The diffraction data were normalized to allow for variations in the incident flux, corrected for detector dead time, beam polarization, background scattering effects (including those from the sample container), absorption and variation of the illuminated sample volume, with

analysis based on that described by Warren [40]. As for the case of neutron diffraction, inelastically scattered x-rays affect the data quite considerably. Again, a method of smooth curve fitting is applied until the data oscillate about the calculated self-scattering profile, which is then subtracted to leave the interference function. From this the structure factor, $S(Q)$, can be obtained. The $S(Q)$ produced is in electron units, and by Fourier transformation to $G(r)$, interatomic distances can be determined. Unlike those for the neutron diffraction data, the weighting coefficients in the x-ray $G(r)$ are monotonically dependent on the atomic number, Z. Thus, for example, a pair distribution function for a-C:H obtained from x-ray diffraction will approximate to the partial $g_{CC}(r)$.

2.4. Infrared spectroscopy

IR measurements were performed using a Fourier transform infrared spectrometer (model Digilab 896). Given the intrinsic difficulties associated with any attempt to analyse IR data quantitatively, we here concentrate on using Gaussian peak fits to the fundamental C–H stretch modes to examine the overall nature of the hydrogen bonding environment and its variation between the different samples. Following a 'background subtraction' using a low-order polynomial, each spectrum was fitted with a series of Gaussians to obtain peak positions. These Gaussian fits are based on the known vibrational frequencies: 2850 cm^{-1} sp^3 CH_2 (symmetric), 2884 cm^{-1} sp^3 CH_3 (symmetric), 2925 cm^{-1} sp^3 CH_2 (asymmetric), 2967 cm^{-1} sp^3 CH_3 (asymmetric), 2887 cm^{-1} sp^3 CH and $\sim$3000 cm^{-1} and above sp^2 CH. Using these peak positions (with a small variation permitted), and allowing free variation of the peak widths and heights, a fit to the data for sample 1 (no H_2 dilution) was obtained. Now, because we are looking at two samples containing similar chemical species and because the two spectra are expected to be consistent, we use the parameters for sample 1 to obtain the fit to the data for sample 2. So, for the hydrogen-diluted sample (sample 2) we fix the peak positions and widths from the fit to sample 1, but allow free variation of the peak heights. This is an entirely reasonable procedure given the chemical similarity of the H bonding environments present in the two samples.

3. Results

3.1. Compositional analysis

From the results of combustion analysis, as shown in table 1, we can see that diluting the pure acetylene precursor gas to a 1:1 mixture of acetylene and hydrogen results in a compositional change from a-C_{77}:H_{23} to a-C_{79}:H_{21}, i.e. causes a small decrease in the hydrogen content of the sample.

3.2. Neutron and x-ray diffraction

The total structure factors and pair correlation functions obtained from the diffraction measurements are shown in figures 1 and 2, respectively. The range of the data in Q-space has a significant effect on the achievable real-space resolution ($\Delta r = 2\pi/Q_{max}$): the neutron $G(r)$ data, derived from $S(Q)$ spectra, where $Q_{max} \sim 50$ $Å^{-1}$, showing much higher resolution ($\sim$0.1 Å) than that obtained in the corresponding x-ray experiments ($\Delta r \sim 0.4$ Å). However, note that at any given Q-value the Q-space resolution of the x-ray data is greater than that achieved in the neutron diffraction experiments (i.e. any sharp, Bragg-like features associated with crystalline inclusions would be more easily detected

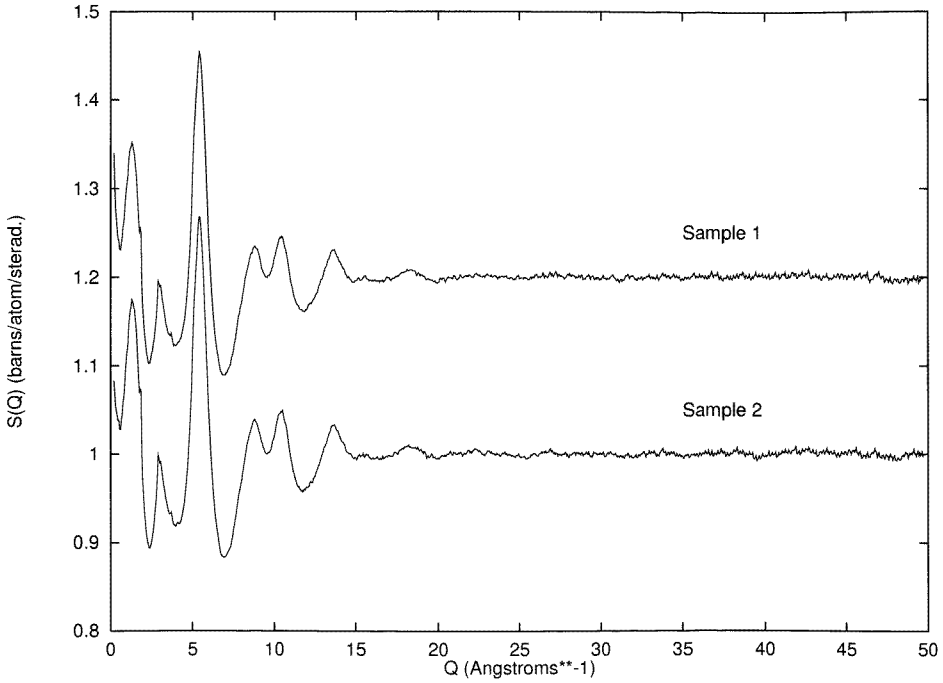

(a)

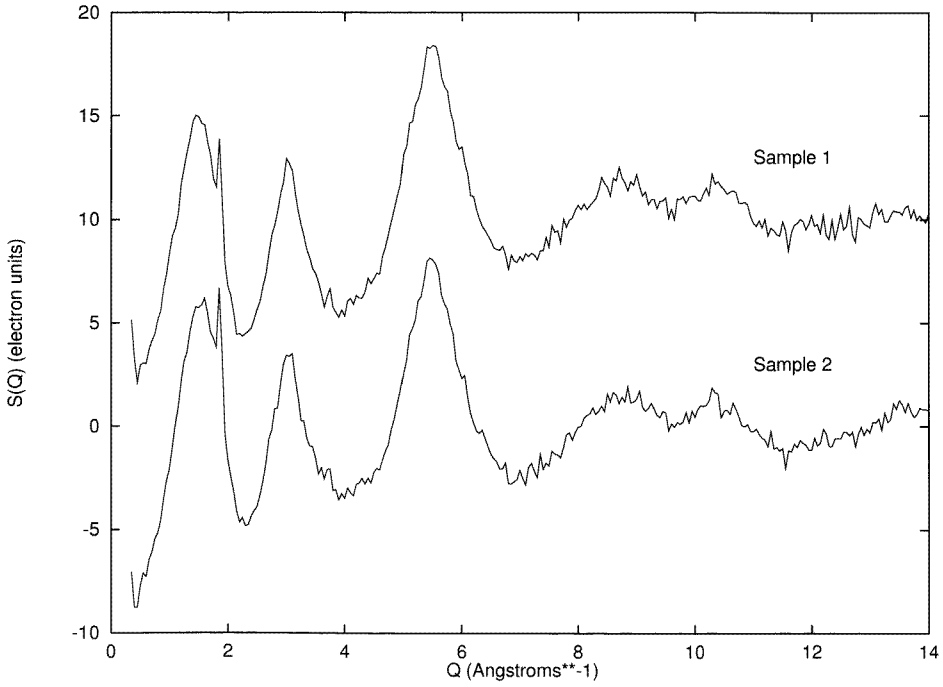

(b)

Figure 1. (a) Structure factors for the two samples obtained from neutron diffraction data, where the incoherent scattering has been subtracted (offset for clarity). (b) Structure factors for the two samples obtained from x-ray diffraction data (offset for clarity).

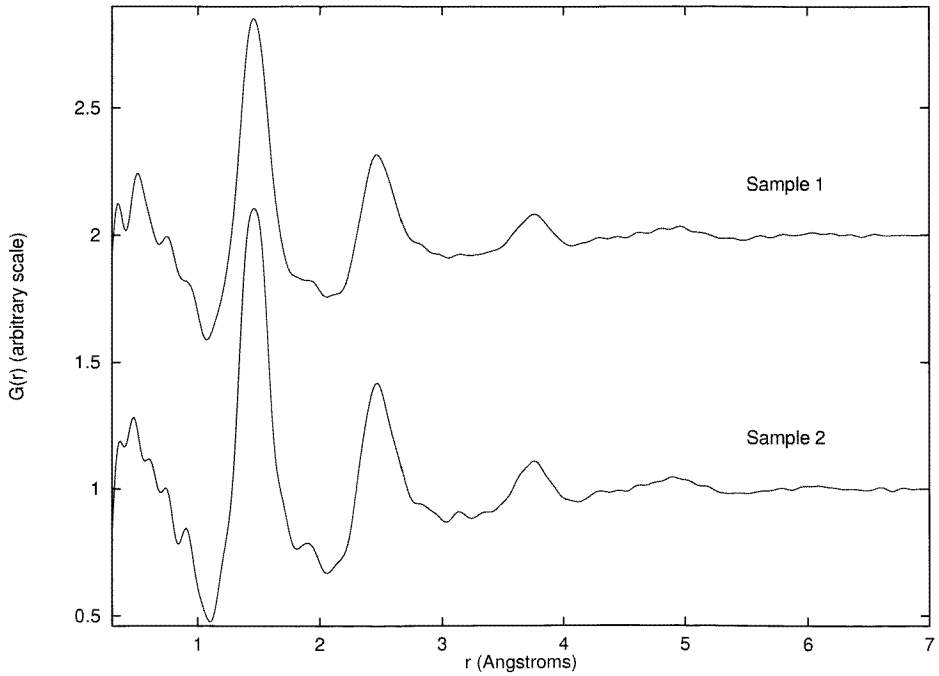

(a)

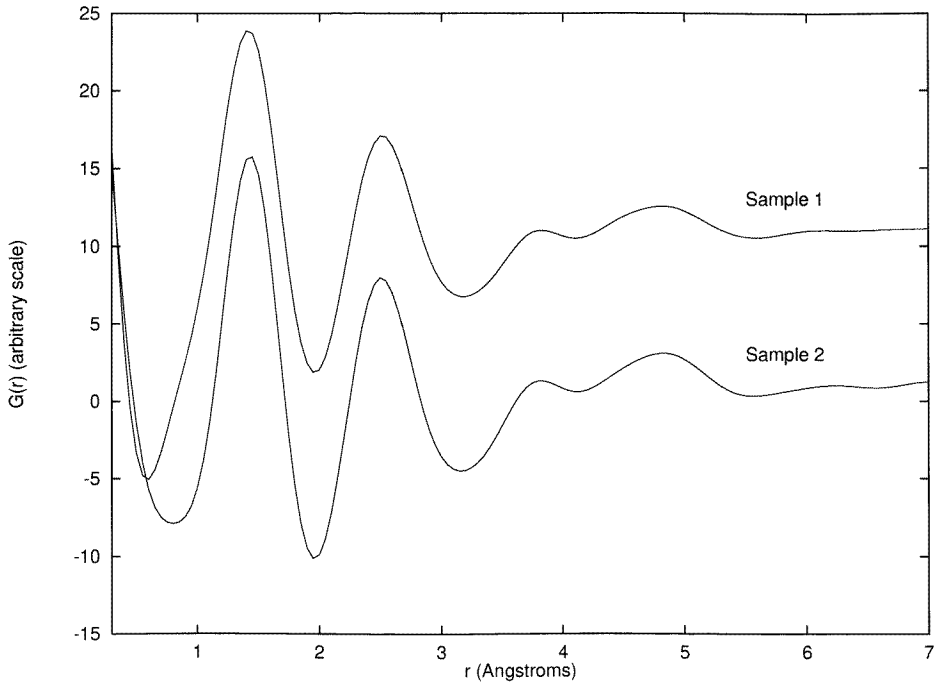

(b)

Figure 2. (a) Pair distribution functions for the two samples obtained from neutron diffraction data (offset for clarity). (b) Pair distribution functions for the two samples obtained from x-ray diffraction data (offset for clarity).

using the x-ray diffractometer). Also, comparing the real-space functions from the neutron and x-ray experiments, we note as expected that correlations involving H are not seen in the x-ray data.

In order to obtain quantitative information, such as peak widths and positions, the real-space functions can be fitted with Gaussians, allowing both position and area to vary. We have fitted the main first-neighbour (∼1.4 Å) and second-neighbour (∼2.4 Å) peaks, together with features either side to improve the accuracy. The results of the Gaussian fitting are given in table 2.

Table 2. Results of the Gaussian fitting of the diffraction data.

	First-neighbour peak position (±0.01 Å)		First-neighbour peak width FWHM (±0.01 Å)	Second-neighbour peak position (±0.01 Å)	
Sample	Neutron	X-ray	Neutron	Neutron	X-ray
1	1.46	1.43	0.10	2.45	2.51
2	1.46	1.44	0.10	2.46	2.50

Consider first of all the total structure factors obtained by neutron diffraction measurements (figure 1(a)). For both of the samples, the oscillations have decayed to the level of the counting statistics by ∼30 $Å^{-1}$, indicating a relatively large degree of variation in the short-range ordering (compared, for instance, to that for a prototypical amorphous network such as silica). The $S(Q)$s are very similar; in fact the small differences are not in the peak positions, but in their relative intensities. Differences in peak shapes and relative intensities are also observed in the x-ray diffraction data (figure 1(b)). One feature of note in these $S(Q)$s is the single, small Bragg-like peak at 1.9 $Å^{-1}$: this has been seen in some previous experimental data for a-C:H [12, 41]. This position is consistent with the well-known graphite interlayer peak (1.92 $Å^{-1}$), although no other bulk graphite-related peaks are observable in the data.

In order to understand what some of these differences mean in terms of structural changes, it is necessary to look at the Fourier-transformed data, the total pair correlation functions $G(r)$.

For both the neutron (figure 2(a)) and x-ray (figure 2(b)) real-space functions, the dominance of the sp^2 CC bonding environment and the insufficient quantity of sp^3 CC bonds (1.54 Å) means that it is not possible to observe directly the different CC single and double bond lengths, and they merge to form a broad peak at ∼1.4 Å. The same is also true for their second-neighbour correlations at ∼2.5 Å. For correlations involving hydrogen, the neutron diffraction data show a definite negative-going region at ∼1.0–1.1 Å assigned to C–H, and there is a possibility that some samples show a small H–H peak at ∼0.8 Å, but this is no more significant than other small peaks at lower r-values and therefore cannot here be taken as definite evidence for the presence of H_2 molecules; cf. [6, 23].

By considering the Gaussian-fitting results (table 2), we may examine in detail the changes in structure that are occurring. For sample 1 the positions of the first-neighbour CC peak are 1.46 Å and 1.43 Å for the neutron and x-ray data, respectively; the CC first-neighbour bond distances obtained from the x-ray data are consistently shorter than the corresponding values from the neutron data. This may be a reflection of the fact that the x-rays scatter from the electron distributions, rather than from the nuclei, which are certainly not spherical in a covalent bond, but is at least as likely to be due to systematic error in the

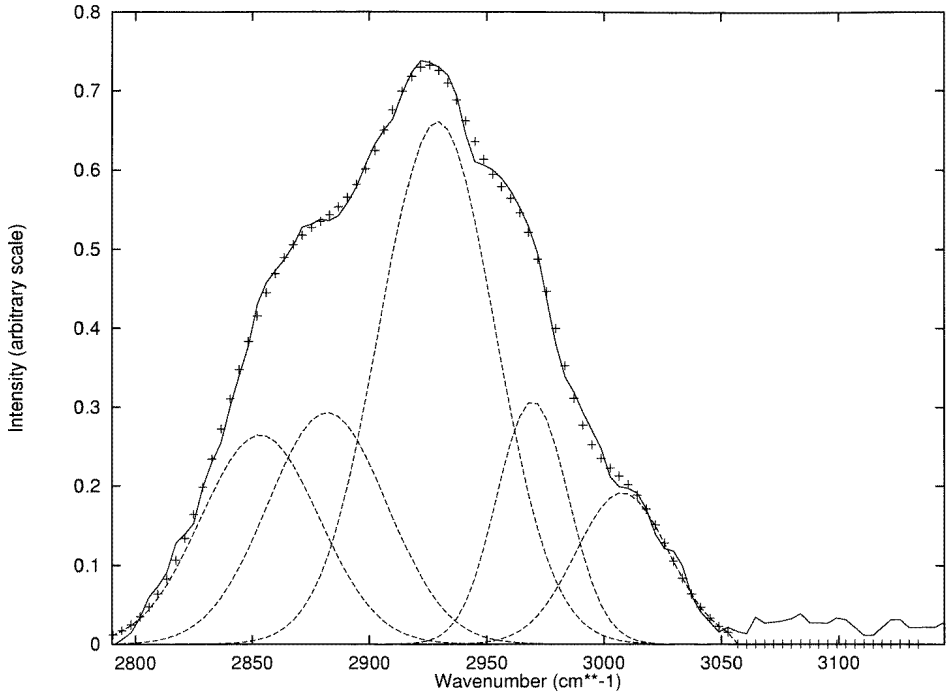

(a)

Figure 3. (a) Infrared spectra in the region 2800–3150 cm^{-1} for sample 1 showing the individual Gaussians used to fit the data. Experimental data are shown as the solid line, the total fit by the crosses (+) and the individual Gaussians are the dashed lines. (b) Infrared spectra in the region 2800–3150 cm^{-1} for sample 2 showing the individual Gaussians used to fit the data. Experimental data are shown as the solid line, the total fit by the crosses (+) and the individual Gaussians are the dashed lines.

data analysis processes associated with corrections for the self-scattering/Compton profiles. We take the values from the more straightforwardly determined neutron diffraction data to be closest to the actual bond lengths. The CC peak at 1.46 Å shows little asymmetry, and the position is consistent with sp^2 being the dominant carbon bonding environment. However, we are unable to determine whether the sp^2 environment is olefinic, aromatic or graphitic. If the bonding is graphitic, then the absence of Bragg-like features indicates that it is disordered, i.e. it is *not* microcrystalline. On the low-r side of this peak, the C–H dip is observed at ∼1.1 Å, and on the high-r side (∼1.8 Å) features corresponding to H–C–H (positive) and C–C–H (negative) correlations are seen. The main second-neighbour peak at ∼2.5 Å is due to C–C–C correlations. The positions of these features remain unchanged between the two samples. Using the first- and second-neighbour CC and CCC distances, we can determine the average CCC bond angle: the value obtained for both samples is 115°. This indicates that the average carbon bonding environment is intermediate between tetrahedral and graphitic bonding.

Diluting the precursor gas with hydrogen does not result in any dramatic changes in the average structure of the film. Indeed, from the results of the Gaussian fitting of the data given in table 2, it is clear that the similarity in the average structure of the samples exists at a quantitative level. There are small differences in peak positions on the addition of

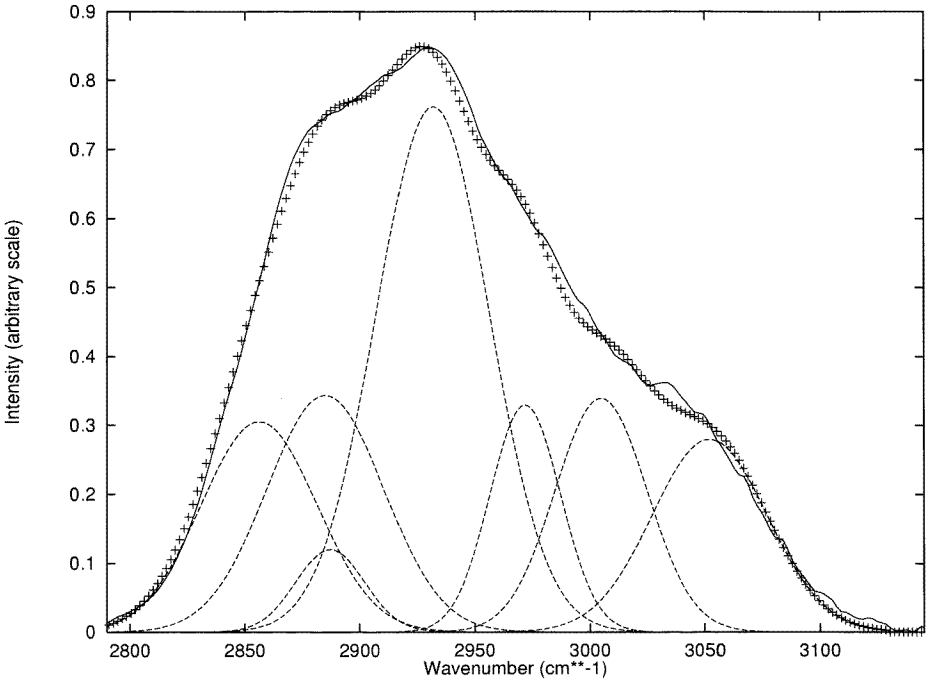

(b)

Figure 3. (Continued)

hydrogen to the precursor gas, but these can all be considered to be within the experimental errors. However, between the main CC and CCC peaks at ∼1.9 Å lie the H–C–H and C–C–H correlations. The first of these is positive and the second negative, and it is evident that in this region the neutron diffraction data for the two samples show a small difference (see figure 2(a)). For the sample with hydrogen dilution (sample 2), both features in this region are slightly more pronounced and narrower than for the undiluted sample. However, it may be the case that the enhancement of only one of the correlations makes it appear that both are changed: for example, if the C–C–H feature becomes more negative, it may appear that the H–C–H feature is more positive. Therefore, a detailed description of the structural changes involved is not possible from these data alone.

In summary, the neutron and x-ray diffraction data show that, in terms of the average structure of the two samples, i.e. average bond lengths and angles, diluting the precursor gas with 50% hydrogen has no observable effect. However, small differences between the two samples are observed in the second-neighbour H–C–H and/or C–C–H correlations.

3.3. Infrared spectroscopy

The most useful region of the IR spectra is the CH stretch which extends from ∼2800 to 3100 cm^{-1}, and is shown in figure 3 together with the Gaussians used to obtain the fits for each sample. From the positions of the Gaussians, assignment of the observed frequencies to vibrational modes can be made and the peak areas can be normalized to the hydrogen content of the sample and used to look at the relative proportions of each mode present in the samples. Table 3 gives the frequencies and associated normalized peak areas derived

Table 3. Results of the Gaussian fitting of the infrared data.

Sample	H_2 dilute?	Peak position (± 3 cm^{-1}) *Normalized peak area (± 0.005)*						
1	No	2853 *0.17*	2882 *0.19*		2929 *0.42*	2969 *0.12*	3007 *0.10*	
2	Yes	2856 *0.14*	2884 *0.16*	2887 *0.03*	2932 *0.33*	2972 *0.09*	3005 *0.12*	3052 *0.12*
Assignment		sp^3 CH_2 (symmetric)	sp^3 CH_3 (symmetric)	sp^3 CH	sp^3 CH_2 (asymmetric)	sp^3 CH_3 (asymmetric)	sp^2 CH	sp^2 CH

from these data, together with the peak assignments. It is important to remember that these values are not absolutely normalized and comparisons are only meaningful in a relative way between samples.

Before discussing the results in detail, it is worth pointing out that although frequencies associated with sp^2 CH_2 groups are not observed (they are not clearly observed in IR spectra for a-C:H in general [42–44]), this is due to the weightings of their matrix elements and does not necessarily imply that these groups are absent. From figure 3 and table 3, it is clear that five of the frequency assignments made are common to both of the samples, although sample 2 has an additional bands at $\sim$2887 cm^{-1} and $\sim$3050 cm^{-1}.

Looking at the values given in table 3, the first and most obvious point to make is that there are significant differences in the bonding environments of hydrogen between the two samples. Indeed, the dilution of the precursor gas with hydrogen results in the emergence of two additional bands, sp^3 CH ($\sim$2887 cm^{-1}) and aromatic sp^2 CH ($\sim$3052 cm^{-1}), and an overall decrease in the number of sp^3 CH_2 and CH_3 groups. Since the diffraction data show no measurable change in the relative quantities of sp^2 and sp^3 sites, the increase in CH groups must be correlated with the reduction in sp^3 CH_2 and CH_3 content; either by further hydrogenation, or by preferential etching by H during deposition. Note that the trends observed in the symmetric and antisymmetric bands are consistent.

These results can also be used to clarify the changes observed in the diffraction data, which shows small differences in the H–C–H and/or the C–C–H correlations on hydrogen dilution. These changes are now seen to be due to a large decrease in the number of sp^3 and sp^2 CH groups, which will result in an increase in the number of C–C–H correlations, thereby resulting in a more negative feature in the neutron diffraction data, which will also give the appearance of an enhanced H–C–H feature.

4. Discussion

Both the diffraction and spectroscopy data-sets show that the most significant effect of diluting the acetylene precursor gas with 50% hydrogen is to increase the number of CH (and therefore also C–C–H) correlations, whilst reducing the number of sp^3 CH_3 and sp^3 CH_2 groups. (There is no information from the IR spectroscopy data on sp^2 CH_2 groups.) Also, a second, aromatic sp^2 CH frequency is seen in the hydrogen-diluted sample.

From the results of combustion analysis (table 1) we know that the hydrogen contents of the two samples are approximately the same, so an increase in sp^3 CH and sp^2 CH groups is not simply the result of more hydrogen being incorporated into the material. Also, both neutron and x-ray diffraction measurements show that there are no observable

differences in the average bond lengths and angles between the samples, which tells us that the basic carbon network and the ratio of CC bond types is unaffected by hydrogen dilution. Therefore, during the film deposition process, the additional hydrogen provided by dilution of the precursor gas is primarily affecting the hydrogen bonding environments, and is not interfering with the formation of the carbon network to any observable extent.

From the IR data, the changes in the hydrogen bonding environment are similar to those observed for high hydrogen dilution (>80%) of amorphous silicon compounds [15, 16, 19], i.e. a decrease in the di/polyhydride fraction and an increase in the monohydride content. The relative changes in these a-C:H samples are not as large, but they are certainly significant, and it is likely that the additional hydrogen in the deposition process acts in the same way. In the formation of amorphous silicon materials, it is thought that the hydrogen covers the growing surface, increasing the mobility of the adsorbed species and resulting in a more relaxed network with fewer microvoids. The diffraction data show no observable change in the network structure, but the decrease in the number of sp^3 CH_n ($n \geqslant 2$) implies a lower microvoid fraction. However, such is the diversity of bonding conformations available to carbon that it is not difficult to visualize a model whereby the network contains fewer microvoids, but the average interatomic correlations are not affected. Small-angle scattering could prove useful in this context by characterizing any changes on the mesoscopic scale. The increased surface mobility could partially explain the reduced number of di/polyhydride groups in our hydrogen-diluted sample. Hydrogen is a network terminator and therefore di/polyhydride groups require the network to 'grow' around them, forming a microvoid. If the surface atoms are more mobile, it is probable that instead of hydrogen saturating dangling bonds to form these di/polyhydride groups, mobile carbon atoms will be able to migrate quickly across the surface and form chemical bonds themselves, thereby resulting in the formation of a more continuous network. Overall, this means that the incorporated hydrogen will be more evenly distributed throughout the network as monohydride groups. In this way the number of C–H bonds is unchanged. In fact, the only difference will be in the number of H–C–H and C–C–H correlations, where the first decreases and the second increases.

However, this is not the only process which is occurring, and the explanation of the changes observed on dilution of the precursor gas with hydrogen is unlikely to be straightforward. In addition to increasing the mobility on the growth surface, in CVD diamond film growth [13] it is accepted that hydrogen can affect the growing film by a combination of chemical bonding to passivate dangling bonds, preferential etching of certain carbon sites (notably the sp^2 sites in diamond/hard a-C:H deposition) and chemical etching of hydrogen. The results presented here are consistent with the dominant process being chemical etching of H from sp^3 CH_2 and CH_3 groups by H in the plasma. This could also result in the large increase in CH groups which is observed. It is probable that a combination of increased surface mobility and chemical etching results in the changes observed between these two samples, with the other processes mentioned above playing only minor roles in the deposition.

The other major change in bonding which can be seen from the IR spectroscopy data also concerns the sp^2 CH groups. In the hydrogen-diluted sample there are clearly two sp^2 CH bonding environments: $\sim$3005 cm^{-1} corresponding to olefinic sp^2 CH stretching, and the second at $\sim$3050 cm^{-1} which is assigned to aromatic sp^2 CH stretching. The first band is seen in both samples, but the second is only found in the hydrogen-diluted sample. However, the diffraction data have shown that there are no changes in the average C network. This means that although no aromatic CH stretching band appears in the spectrum for sample 1, that does not mean that there are no aromatic groups in the sample: they are

there, but are unhydrogenated. So, we are not seeing a transformation of the sp^2 carbon bonding environment from olefinic to aromatic, but rather a hydrogenation of the aromatic fraction. Note that the diffraction data show no evidence for extended aromatic clusters. The hydrogenation of these groups could well be a result of the higher hydrogen content of the precursor gas. The samples have approximately the same hydrogen content; however, the number of sp^3 CH_2 and CH_3 groups decreases by a large fraction. If the balance is to be maintained then, for example, for every CH_2 group lost, two CH groups should be created. This means that there is more H available for bonding to the aromatic C. In the undiluted sample, this H is 'taken' by the sp^3 CH_2 and CH_3 groups.

PVD/CVD-deposited a-Si:C:H is a rather different material, and it is interesting to note that H_2 dilution of the precursor gas mixture leads to somewhat different changes in that the concentration of SiH_2 is seen to grow at the expense of SiH [20]. Indeed, the nature of the gas mixture is of importance in other respects in the a-Si:C:H case since the Si:C ratio correlates with the microvoid content and conformation through the Si/C–H_3 concentrations present in the material. These act as network terminators and thereby promote the formation of voids as the network grows around the unit [45]; this in turn controls the photo-oxidation process that is central to the material's potential in lithography.

With reference to our base-line model for a-C:H outlined above, the effect of hydrogen dilution on the carbon network can be seen as increasing the volume fraction of protonated carbons without altering the single:double-bond ratio significantly. NMR studies using a suite of techniques could provide important additional information in this context: the different spin–lattice relaxation behaviour associated with the various hydrogen sites provides a means of spectral editing of cross-polarization magic-angle spinning, combined rotation and multiple-pulse spectroscopy, dipolar dephasing spectra and multiple quantum experiments.

5. Conclusions

We have investigated the effects of diluting the acetylene precursor gas in a fast-atom beam deposition process with 50% hydrogen on the structure of a-C:H, using neutron and x-ray diffraction and infrared spectroscopy. The diffraction results show that there is no observable change in the average structure of the material i.e. the average bond distances and angles. However, the infrared spectra show that there are significant changes in the bonding environment of hydrogen within the network. Dramatic increases in the sp^2 CH and sp^3 CH content are seen, together with a decrease in the number of sp^3 CH_2 and CH_3 groups. These effects are attributed to changes in the deposition process caused by the presence of extra hydrogen, and can be mostly put down to increased mobility of adsorbed species on the surface of the growing film, and the preferential etching of bonded H by H in the plasma. These data also illustrate the need for complementary experimental data in these kinds of structural investigation. Given the diffraction data alone, the conclusion would have been that the hydrogen dilution has no effect on the atomic-scale structure of a-C:H; however, we know that, as far as the hydrogen is concerned, this is not the case at all.

Acknowledgments

We would like to thank A Fassam (Chemistry, UKC) for carrying out the combustion analysis and D T Bowron for his help and the use of his programs for analysis of the x-ray

diffraction data. JKW acknowledges the financial support of the Royal 1851 Commission. The experimental work was supported by the EPSRC.

References

[1] Angus J C, Koidl P and Domitz S 1986 *Plasma Deposited Thin Films* ed J Mort and F Jansen (Boca Raton, FL: Chemical Rubber Company Press) ch 4, p 89
[2] Robertson J 1986 *Adv. Phys.* **35** 317
[3] Lettington A H 1991 *Diamond and Diamondlike Films and Coatings* ed J C Angus, R E Clausing, L L Horton and P Koidl (New York: Plenum) p 481
[4] Aisenberg S and Kimock F M 1989 *Mater. Sci. Forum* **52+53** 1
[5] Robertson J 1991 *Prog. Solid State Chem.* **21** 199
[6] Honeybone P J R, Newport R J, Howells W S, Tomkinson J and Revell P J 1991 *Chem. Phys. Lett.* **180** 145
[7] Jäger C, Gottwald J, Spieß H W and Newport R J 1994 *Phys. Rev.* B **50** 846
[8] Walters J K and Newport R J 1995 *J. Phys.: Condens. Matter* **7** 1755
[9] Kleber R, Weiler M, Krügler A, Sattel S, Kunz G, Jung K and Ehrhardt H 1993 *Diamond Relat. Mater.* **2** 242
[10] Lifshitz Y, Kasi S R and Rabalais J W 1989 *Mater. Sci. Forum* **52+53** 237
[11] Veerasamy V S, Amaratunga G A J, Milne W I, Robertson J and Fallon P J 1993 *J. Non-Cryst. Solids* **164–166** 1111
[12] Walters J K, Algar C D, Burke T M, Rigden J S, Newport R J, Bushnell-Wye G, Howells W S and Sattel S 1996 *J. Non-Cryst. Solids* **197** 41
[13] Robertson J 1994 *Diamond Relat. Mater.* **3** 361
[14] Olson D S, Kelly M A, Kapoor S and Hagstrom S B 1993 *J. Appl. Phys.* **74** 5167
[15] Middya A R, Ray S, Jones S J and Williamson D L 1995 *J. Appl. Phys.* **78** 4966
[16] Hazra S, Middya A R and Ray S 1996 *J. Phys. D: Appl. Phys.* **29** 1666
[17] Rocheleau R E, Zhang Z, Niles D W and Mason A 1992 *J. Appl. Phys.* **72** 282
[18] Okamoto S, Hishikawa Y and Tsuda S 1996 *Japan. J. Appl. Phys.* **35** 26
[19] Alvarez F, Sebastiani M, Pozzilli F, Fiorini P and Evangelisti F 1992 *J. Appl. Phys.* **71** 267
[20] Honeybone P J R, Walters J K, Newport R J, Howells W S and Tomkinson J 1994 *J. Non-Cryst. Solids* **169** 54
[21] Paterson M J, Orrman-Rossiter K G, Sood D K and Bhargava S K 1993 *Diamond Relat. Mater.* **2** 1439
[22] Tsai H 1989 *Mater. Sci. Forum* **52+53** 71
[23] Walters J K, Honeybone P J R, Huxley D W, Newport R J and Howells W S 1994 *Phys. Rev.* B **50** 831
[24] Johnson P A V, Wright A C and Sinclair R N 1983 *J. Non-Cryst. Solids* **58** 109
[25] Gaskell P H, Saeed A, Chieux P and McKenzie D R 1992 *Phil. Mag.* B **66** 155
[26] Dischler B 1987 *Amorphous Hydrogenated Carbon Films* ed P Koidl and P Oelhafen (Paris: Les Editions de Physique) p 189
[27] Angus J C, Stultz J E, Shiller P J, MacDonald J R, Mirtich M J and Domitz S 1984 *Thin Solid Films* **118** 311
[28] Vandentrop G J, Kawasaki M, Kobayashi K and Somorjai G A 1991 *J. Vac. Sci. Technol.* A **9** 1157
[29] Walters J K, Fox D M, Burke T M, Weedon O D, Newport R J and Howells W S 1994 *J. Chem. Phys.* **101** 4288
[30] Walters J K, Newport R J, Howells W S and Parker S F 1995 *J. Phys.: Condens. Matter* **7** 10 059
[31] Franks J 1984 *Vacuum* **34** 259
[32] Franks J 1989 *J. Vac. Sci. Technol.* A **7** 2307
[33] Boland B and Whapham S (ed) 1992 ISIS User Guide—Experimental Facilities *Rutherford Appleton Laboratory Report* RAL-92-041
[34] Newport R J 1988 *Neutron Scattering at a Pulsed Source* ed R J Newport, B D Rainford and R Cywinski (Bristol: Hilger) ch 13, p 233
[35] Squires G L 1978 *Introduction to the Theory of Thermal Neutron Scattering* (Cambridge: Cambridge University Press)
[36] Gunn J M F 1988 *Neutron Scattering at a Pulsed Source* ed R J Newport, B D Rainford and R Cywinski (Bristol: Hilger) ch 1, p 5
[37] Howells W S, Soper A K and Hannon A C 1989 ATLAS—analysis of time-of-flight diffraction data from liquid and amorphous samples *Rutherford Appleton Laboratory Report* RAL-89-046
[38] Placzek G 1952 *Phys. Rev.* **86** 377

[39] Turner J Z and Soper A K 1995 *SANDALS Survival Guide* unpublished
[40] Warren B E 1990 *X-ray Diffraction* (New York: Dover)
[41] Walters J K, Newport R J, Howells W S and Bushnell-Wye G 1996 *J. Phys.: Condens. Matter* **8** 4739
[42] Lukins P B, McKenzie D R, Vassallo A M and Hanna J V 1993 *Carbon* **31** 569
[43] Dischler B, Bubenzer A and Koidl P 1983 *Solid State Commun.* **48** 105
[44] González-Hernández J, Chao B S and Pawlik D A 1989 *Mater. Sci. Forum* **52+53** 543
[45] Rigden J S, Algar C D, Newport R J, North A N, Ibrahim F and Wilson J I B 1994 *J. Non-Cryst. Solids* **190** 54